International Journal of Nanomedicine

Dovepress
open access to scientific and medical research

Open Access Full Text Article

ORIGINAL RESEARCH

3D-HA Scaffold Functionalized by Extracellular Matrix of Stem Cells Promotes Bone Repair

This article was published in the following Dove Press journal:
International Journal of Nanomedicine

Hui Chi[1]
Guanghua Chen[1]
Yixin He[2]
Guanghao Chen[1]
Hualei Tu[3]
Xiaoqi Liu
Jinglong Yan[1]
Xiaoyan Wang[1]

[1]Department of Orthopedics, The Second Affiliated Hospital of Harbin Medical University, Harbin, People's Republic of China; [2]Department of Nephrology, The Second Affiliated Hospital of Harbin Medical University, Harbin, People's Republic of China; [3]Department of Burn, The Fifth Hospital of Harbin Medical University, Harbin, People's Republic of China

Background and Purpose: The extracellular matrix (ECM) derived from bone marrow mesenchymal stem cells (BMSCs) has been used in regenerative medicine because of its good biological activity; however, its poor mechanical properties limit its application in bone regeneration. The purpose of this study is to construct a three dimensional-printed hydroxyapatite (3D-HA)/BMSC-ECM composite scaffold that not only has biological activity but also sufficient mechanical strength and reasonably distributed spatial structure.

Methods: A BMSC-ECM was first extracted and formed into micron-sized particles, and then the ECM particles were modified onto the surface of 3D-HA scaffolds using an innovative linking method to generate composite 3D-HA/BMSC-ECM scaffolds. The 3D-HA scaffolds were used as the control group. The basic properties, biocompatibility and osteogenesis ability of both scaffolds were tested in vitro. Finally, a critical skull defect rat model was created and the osteogenesis effect of the scaffolds was evaluated in vivo.

Results: The compressive modulus of the composite scaffolds reached 9.45±0.32 MPa, which was similar to that of the 3D-HA scaffolds ($p>0.05$). The pore size of the two scaffolds was 305±47 um and 315±34 um ($p>0.05$), respectively. A CCK-8 assay indicated that the scaffolds did not have cytotoxicity. The composite scaffolds had good cell adhesion ability, with a cell adhesion rate of up to 76.00±6.17% after culturing for 7 hours, while that of the 3D-HA scaffolds was 51.85±4.77% ($p<0.01$). In addition, the composite scaffold displayed higher alkaline phosphatase (ALP) activity, osteogenesis-related mRNA expression, and calcium nodule formation, thus confirming that the composite scaffolds had good osteogenic activity. The composite scaffolds exhibited good bone repair in vivo and were superior to the 3D-HA scaffolds.

Conclusion: We conclude that BMSC-ECM is a good osteogenic material and that the composite scaffolds have good osteogenic ability, which provides a new method and concept for the repair of bone defects.

Keywords: bone tissue engineering, extracellular matrix, stem cells, 3D printed scaffold, osteogenesis

Introduction

Currently, the application of tissue engineering technology in bone repair is a hot topic in the field of regenerative medicine, and the three key components are tissue-engineered scaffolds, seed cells and the osteoblastic environment.[1] Tissue-engineered scaffolds are the core component, and effective bone tissue-engineered scaffolds should have the following characteristics: excellent osteogenic ability, sufficient mechanical strength, and appropriate pore size and porosity.[2,3] With excellent osteogenic ability, seed cells can differentiate into osteoblasts to promote bone regeneration. With sufficient mechanical strength, the scaffolds can play a supporting role at the bone defect and bear a certain

Correspondence: Xiaoyan Wang; Jinglong Yan
Department of Orthopedics, The Second Affiliated Hospital of Harbin Medical University, 246 XueFu Road, Harbin, Heilongjiang Province, People's Republic of China
Email wxyg7@hrbmu.edu.cn; yanjinglongg6@126.com

submit your manuscript | www.dovepress.com
DovePress
http://doi.org/10.2147/IJN.S259678

amount of stress. According to the classical Wolf law, stress will further promote osteogenesis.[4–6] With the appropriate pore size and porosity, the seed cells can enter and adhere to the scaffolds to promote osteogenesis. However, it is difficult for a single material to meet all these requirements; therefore, the combined application of materials is currently a popular approach.

Various kinds of materials and strategies have been employed to construct the scaffold, and the relevant materials include natural or synthetic polymers, bioceramics and peptide-based materials.[7] In recent years, extracellular matrix (ECM) has received more attention due to its good activity and biocompatibility. It is a protein polypeptide complex secreted by cells and plays important roles in cell proliferation, differentiation, metastasis, and cell interactions.[8–10] Stem cells first secrete ECM, which accumulates and matures to form a three-dimensional network structure with abundant organic components, and these components allow the ECM to promote multidirectional differentiation and be applied in tissue regeneration.[11] However, the mechanical properties of BMSC-ECM are poor and the scaffolds produced are not strong enough; therefore, they can only serve as fillers and cannot provide effective support when applied in vivo, thereby limiting their application in bone regeneration.[1]

It is necessary for the scaffold to provide 3D cell-growth microenvironments and appropriate synergistic cell-guidance cues to mimic native tissues. Therefore, 3D scaffolds exhibit several advantages when compared to 2D scaffolds, including high surface-to-volume ratio, 3D porous structure, favorable mechanical characteristics, etc., which are beneficial to cell attachment, proliferation, oxygenation/nutrient up-take, waste excretion, homogeneous/isotropic growth of tissues and cell–cell interactions.[12] Hydroxyapatite (HA) is the most common type of calcium phosphate, which is the main inorganic component in human bone tissue. After implantation, calcium and phosphorus dissociate from the material surface are absorbed by body tissues, and grow into new tissues.[13] Due to the growing maturity of bioprinting technology, researchers have produced 3D-printed HA scaffolds with sufficient mechanical strength and reasonably distributed spatial structure.[14,15] However, HA is limited by the weak osteogenic ability, and surface modification is one such strategy to solve this problem, the active ingredients with HA scaffolds are often combined via transgenic methods to improve the osteogenic ability of the scaffolds.[16–19] However, a single component cannot simulate the complex composition of the ECM and the interactions among various macromolecules; therefore, the application effect is still not as good as that of a complete ECM.[20,21]

Therefore, BMSC-ECM has excellent osteogenic ability, while the 3D-HA scaffolds have sufficient mechanical strength and a reasonably distributed spatial structure. The composite scaffolds formed by combining 3D-HA scaffolds and BMSC-ECM can meet all the characteristics of functional scaffolds; however, determining how to combine the two is a key problem. Previous studies indicated that HA can be successfully modified by aminopropyltriethoxysilane (APTES), which makes it possible to conjugate HA with active ingredients.[22,23] Oligonucleotides have two polypeptide chains called anchor strands (NH2-CCAAACCCGTCAATCAAGTCTACACTGTTC) and complementary strands (NH2-CAGTGTAGACTTGATTG ACGGGTTT), with a reverse complementary structure.[24] Therefore, in this study, we combined the two oligonucleotide polypeptide chains with 3D-HA scaffolds and ECM particles and then mixed them at room temperature to obtain 3D-HA scaffolds modified by micron-scale ECM particles on the surface (as shown in Figure 1).

In conclusion, we selected micron-scale BMSC-ECM with good osteogenic ability as the modifying material and combined it with 3D-printed HA scaffolds to generate composite scaffolds with a simple, stable and efficient linking method. The scaffolds have three characteristics at once: excellent osteogenic ability, sufficient mechanical strength and reasonably distributed spatial pore structure. They were tested for their osteogenic ability and potential to provide a new method and concept for bone repair and bone regeneration in vivo and in vitro.

Materials and Methods

Rats

Male Sprague Dawley (SD) rats weighing approximately 250 g were purchased from the Animal Experiment Centre of the Second Affiliated Hospital of Harbin Medical University. All experiments involving animals were approved by the Animal Use and care Committee of Harbin Medical University (approval number: SYDW2018-005) in accordance with guidelines of the US NIH.

Extraction of BMSCs

BMSC extraction was performed as previously described. Male SD rats weighing approximately 50 g were sacrificed by spinal cord dissection. Bilateral femurs were harvested under aseptic conditions, and all muscle tissues were

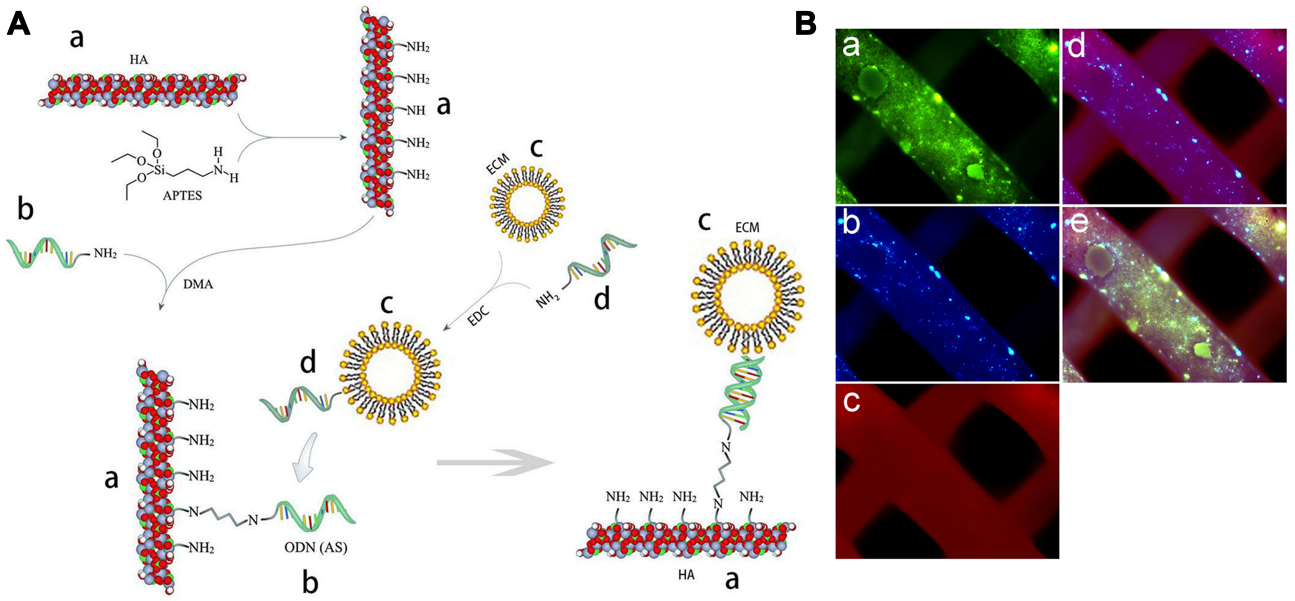

Figure 1 Fabrication of 3D-HA/BMSC-ECM scaffolds via fluorescence labeled modular oligonucleotide immobilization system. (**A**) Schematic illustration of the 3D-HA /BMSC-ECM conjugation. (Aa) 3D-HA scaffolds; (Ab) anchor strands (AS); (Ac) BMSC-ECM; (Ad) complementary strands (CS). (**B**) Fluorescence images. (Ba) Green staining indicates that AS (FITC labeled) are immobilized on the scaffolds surface. (Bb) Identification of the complementary strands staining (AMCA, blue). (Bc) Rhodamine-B labels ECM. (Bd) The overlaid yellow (red + blue) staining indicates that the ECM is connected with the complementary strands. (Be) Image overlaid to show that BMSC-ECM is successfully conjugated onto the 3D-HA scaffolds.

removed. The bone marrow cavity was irrigated with Dulbecco's modified eagle medium (DMEM, HyClone, USA) to obtain a mixture of bone marrow and DMEM. After centrifugation, the precipitate was resuspended in DMEM + bovine serum albumin (BSA, HyClone) + penicillin-streptomycin (Beyotime, Shanghai, China). Culture was conducted for 3 days under the following conditions: 95% humidity, 37°C temperature and 5% carbon dioxide concentration. The nonadherent cells were then removed, and the culture medium was refreshed. After the adherent cells reached 90–95% confluence, the cells were passaged, and the third passage (P3) of stem cells was used for identification and subsequent experiments. The identification method was the same as in a previous experiment, and the identified cells met the stem cell standard.[2]

Preparation of Micron-Scale Extracellular Matrix Suspension

The extraction method for ECM derived from BMSCs is the same as in a previous study.[11] P3 BMSCs were subjected to continued culture under conditions containing ascorbic acid (50 μg/mL) and ascorbate-2-phosphate (150 μg/mL) in a sterile cell culture bottle. After the cells achieved confluence, they were not passaged for 3–4 weeks. The bottom of the bottle was then covered with a transparent membrane, which was the ECM membrane. The supernatant was discarded, 2 mL of trypsin (Beyotime, Shanghai, China) was added, and the bottom of the bottle was tapped to obtain the ECM without cells, which was further formed into a micron suspension (mass ratio 1%) by a tissue homogenizer.

Preparation of the 3D-HA Scaffolds

Polyvinyl alcohol (YANKE, Xiamen, China) solution with a 6% mass ratio was used as an excipient for printed ink. HA granules (YANKE, Xiamen, China) and the excipient solution were generated into printed ink at a mass ratio of 67%. The components were mixed well and placed in a bioprinter (Bio-Architect Pro, Regenovo, China) with a diameter of 500 mm. The 3D scaffolds were printed on a polished silicon wafer (thickness 0.6 mm). The scaffolds had a biomimetic structure with interior overlapping rods and a continuous exterior surface. The printed scaffolds were dried at room temperature for 2 days, heated to 400°C for 1 hour, and then sintered at 1200°C for 2 hours to increase the strength and remove reagent.

Preparation of the 3D-HA/BMSCS-ECM Scaffolds

As described in previous studies,[25,26] APTES (Beyotime, Shanghai, China) was applied to modify the surface of

hydroxyapatite.[22] Briefly, 0.221 g of APTES was added to 100 mL of ethanol solution at a concentration of 90%, and after mixing, the HA scaffolds were immersed in the mixture for 12 hours. Then, double-distilled water (DDW) and methanol (YANKE, Xiamen, China) with a mass ratio of 90% were applied to wash the scaffolds. After being dried in air, the HA scaffolds with NH_2 groups adhered to the surface were obtained. Then, the scaffolds were immersed in the solution containing oligonucleotide anchor chain again, and 100 mol/L dimethyl adipimidate (DMA) (YANKE, Xiamen, China) was added. After 1 hour of reaction on the shaking table, the HA scaffolds with anchor chain were obtained by rinsing three times with TE buffer solution.

Then, a 10 mL micron-sized ECM suspension (mass ratio 1%) was added to the MES buffer solution, constituting a reaction system, and the cross-linker 1-Ethyl-3-(3′-dimethylaminopropyl)carbodiimide/
N-Hydroxysuccinimide (EDC/NHS, YANKE, Xiamen, China) was added to react at room temperature for 15 min. Afterwards, the complementary strand of oligomeric nucleotides was added for 2 hours at room temperature and 2-sulfonium ethanol was added to quench the reaction and obtain the objective complex. The reaction system was separated with a desalination column, and the ECM with complementary strands of oligomeric nucleotides was obtained.

Finally, the two components were combined to produce micron-sized 3D-HA scaffolds modified by ECM. The schematic illustration of the 3D-HA/BMSC-ECM conjugation is shown in Figure 1A.

Scanning Electron Microscopy (SEM) Scans

Scanning electron microscopy (SEM, Hitachi, S-3400n, Japan) was applied to observe the surface and internal structure of the scaffolds. The operation method was as follows. First, the scaffold surface was covered with gold/palladium, the gold-sprayed scaffolds were placed on the workbench, and the scaffold surface and internal area were observed under appropriate magnification. Then, additional software was used to analyse the height of the scaffold surface.

Compressive Modulus of the Scaffolds

The cylindrical scaffolds were placed on a mechanical testing machine (Instron 5943), a 10 N load cell was used, and the scaffolds were continuously pressurized at a strength of 50 N per minute until they could no longer bear the strength. The compressive stress–strain curve is linear until the strain rate reaches 50%, and the compression modulus is the slope at this time. In addition, after the scaffolds were fully immersed in water, the compressive modulus of the scaffolds was measured again for comparison.[27]

Computer Hydrodynamics Analysis

In theory, the internal structure of the 3D-printed scaffolds is uniform; therefore, their hydrodynamics are also uniform and stable. In this part, common freeze-dried Chitosan/Gelatin (C/G) scaffolds were used as the control group to study the hydrodynamics of composite scaffolds, and production method of C/G scaffolds is the same as in a previous study.[2]

As in a previous report,[28] the hydrodynamics of both scaffolds were analysed according to Darcy's law, which is also known as the linear seepage law and was first used to describe the linear relationship between the seepage velocity of water in saturated soil and the hydraulic slope. It is described as $Q=kA\Delta h/l$ and can also be applied to scaffolds, where Q is the seepage flow per unit time (m^3/s), A is the cross-sectional area of the scaffolds, K is the permeability coefficient of the scaffolds, Δh is the pressure difference of the scaffolds, and l is the height of the scaffolds. Thus, a hydrodynamic analysis was performed using DFA software to assess the scaffolds pressure change and fluid flow.

Cytotoxicity

To detect the cytotoxic effect of both scaffolds, the scaffolds were immersed in 10 mL of complete culture medium and soaked at 37°C for 1 day, 3 days and 7 days. After the scaffolds were removed, the mixture solution containing the scaffolds elution was collected. A total of $1x10^4$ P3 BMSCs were placed in 96-well plates and cultured with complete culture medium and the above 6 mixtures. The culture condition was the same as described above. After 3 days, a cell counting kit-8 (CCK-8, Jiancheng, Nanjing, China) was used to detect the overall cell activity and a cell count plate was used to calculate the number of cells. The CCK-8 results and cell counts were used together to evaluate the cytotoxic effect of the scaffolds.

Adhesion Ratio of Scaffolds

Suspension droplets containing $1x10^5$ BMSCs were placed on the surface of the scaffolds to make the liquid inside and the surface of the scaffolds had moderate tension

without leakage. The scaffolds were placed at 37°C, 5% CO_2 and 95% humidity, cultured for 1, 3, 5 and 7 hours, immersed in complete medium and then vibrated slightly to remove the unattached cells. Afterwards, the scaffolds were removed and used in further experiments; in addition, the medium was centrifuged, and the cells were resuspended and counted. The number of cells not adhering to the scaffolds was counted as n_1, and the cell adhesion rate was $(1\times10^5\text{-}n_1)/1\times10^5\times100\%$.

Cytoactivity

BMSCs adhered onto the scaffolds were cultured in conventional complete medium for 3 and 7 days, then labelled by the method of dead/live staining (Jiancheng, Nanjing, China). Briefly, the kit contains two reagents, calcein AM and ethd-1. The former can enter living cells and be hydrolysed into calcein, which is a green fluorescent molecule; the latter cannot enter living cells but can bind to RNA fragments from dead cells to produce red fluorescence. Therefore, the live cells were green and the dead cells were red.

Cell Morphology on the Scaffolds

The morphology of the BMSCs on both scaffolds was evaluated by cytoskeletal staining and SEM. For cytoskeletal staining, after culturing for 3 and 7 days, the cell-scaffolds composites were carefully rinsed three times with PBS, fixed with 4% paraformaldehyde for 15 min, rinsed three times, and permeabilized with 0.5% Triton X-100 for 5 min. Then, the cytoskeleton of the BMSCs was stained with 0.5% rhodamine phalloidin solution (Yi Sheng, Shanghai, China). Finally, the morphology of the cells on both scaffolds could be observed with an inverted fluorescence microscope (LEICA DMI4000B, Germany). The cell-seeded scaffolds were also detected by SEM to analyse the activity and spreading morphology of the BMSCs.

Eluates from Scaffolds Promote Osteogenesis

BMSCs ($1x10^4$) at P3 were plated in 12-well plates and cultured with normal complete medium and a mixture containing normal medium with eluates from different scaffolds, and the medium was refreshed every 3 days. After culturing for 7 days, 14 days and 21 days, 4% paraformaldehyde was used to fix the cells, and then ALP, Alizarin red and von Kossa staining were used to examine osteogenesis. For ALP staining, the BCIP/NBT Alkaline Phosphatase Color Development Kit (Beyotime, Shanghai, China) was used for 30 min, and then the plate was rinsed with PBS several times. For Alizarin red staining, the reagent (Cyagen, Guangzhou, China) was added for 3 min, and the plate was rinsed with PBS several times to remove the residual dye. For Von Kossa staining (Cyagen, Guangzhou, China), the solution was added to the plate, which was then exposed to ultraviolet light for 10 min and flushed with DDW several times to remove the residual dye. Finally, the plates were observed under an inverted microscope.

In vitro Osteogenesis Induction

As mentioned above, after BMSCs adhered to the scaffolds, the cell-scaffold composites were subjected to continued culture with or without osteogenesis induction (OS) (Cyagen, Guangzhou, China), and the medium was refreshed every 3 days until 7 days, 14 days and 21 days. The osteogenic classical protein alkaline phosphatase (ALP) was detected, and marker genes, such as Collagen I (Col I) mRNA, ALP mRNA, osteopontin (OPN) mRNA, osteocalcin (OCN) mRNA and Runt-related transcription factor 2 (Runx-2) mRNA, were also detected.

For the ALP protein, trypsin was first used to isolate cells from the scaffolds, and then the cell membrane was broken via ultrasonication (SONICS Vibra Cell VCX 105, USA). An ALP assay was performed according to the operating instructions. Afterwards, ELISA (Jiancheng, Nanjing, China) was used to measure the OD value and further calculate the U value. The experiment was repeated three times, and a higher U value indicated a greater ALP content in the cells.

For mRNA detection, cells on the scaffolds were isolated as described above, and TRIzol reagent (HaiGene, Harbin, China) was used to extract total RNA. Golden 1st cDNA Synthesis Kit reagent (HaiGene, Harbin, China) was used for the synthesis of cDNA. Real-time PCR assays for mRNA were performed in a Mini-Opticon2 system (MJ) using Golden HS SYBR Green qPCR Mix, and the reaction conditions were as follows: 95°C for 15 min, followed by 45 cycles of 95°C for 10 s and 60°C for 30 s. GAPDH was purchased from HaiGene (Table 1), and other primers were purchased from Genscript. GAPDH was used as an internal control to standardize the cDNA in each sample. Each sample was repeated three times, and the mean was used to calculate the mRNA expression.

Model of Critical Bone Defects in Animals

Male SD rats weighing approximately 250 g were selected, and general anaesthesia was administered by intraperitoneal injection of chloral hydrate. The rats were laid on the operating table in the prone position with

Table 1 Primers for RT-PCR

Gene	Primer Sequence
Col 1-F	5'-CTGAGATGCTCCCTAGACC-3'
Col 1-R	5'-CCCTTGTTAAATAGCACCTTC-3'
ALP-F	5'-TGTAGAAGGAGGTCGTATTG-3'
ALP-R	5'-GAGAATGGAGGTGTAGGATT-3'
OPN-F	5'-ACGATGATGACGACGACGATG-3'
OPN-R	5'-TTGTGTGCTGGCAGTGAAGG-3'
OCN-F	5'-CAGTAAGGTGGTGAATAGACTCCG-3'
OCN-R	5'-GGTGCCATAGATGCGCTTG-3'
Runx2-F	5'-CTTCGTCAGCGTCCTATC-3'
Runx2-R	5'-CTTCCATCAGCGTCAACA-3'
GADPH-F	5'-AACTCCCATTCTTCCACCTTT-3'
GADPH-R	5'-CTCTTGCTCTCAGTATCCTTG-3'

routine disinfection, and a median incision of approximately 3 cm was made. After stripping the soft tissue, a slow electric drill was used to generate a critical bone defect of approximately 5 mm in diameter in the skull. The study animals were divided into three groups based on the implants: the 3D-HA/BMSC-ECM scaffolds group (experimental group, n=6), the 3D-HA scaffolds group (control group, n=6) and the blank group (n=6). During the first 3 days after the operation, 100,000 units of penicillin sodium was injected intraperitoneally to prevent infection, and then the rats were fed under conventional conditions. Micro-CT scanning (Bruker SkyScan 1174v2, Belgium) was performed at the 12th week to detect the osteogenesis effect, and a quantitative analysis of new bone was conducted, and the bone volume/total volume (BV/TV), trabecular number (Tb.N), trabecular separation (Tb.Sp) and trabecular thickness (Tb.Th) were scanned. BV/TV represents the proportion of bone volume in total volume. Tb.N indicates the average number of intersections between bone and non-bone tissue in single length unit (mm) in the region of interest. Tb.Th is the mean thickness of trabecular, while Tb.Sp represents the average width of medullary cavity between the trabecular.

Statistical Methods

All examinations were performed on six replicate samples unless otherwise indicated, and the data are presented as the Mean±SD. SPSS confirmed that all data are in accordance with a normal distribution. An independent-samples *t*-test and one-way analysis of variance (ANOVA) were used to calculate significant differences. $P<0.05$ or 0.01 was considered significant.

Results

Fabrication of 3D-HA/BMSCS-ECM Scaffolds

An immunofluorescence assay was employed to confirm the successful conjugation of 3D-HA scaffolds and BMSC-ECM using a modular oligonucleotide immobilization system. As shown in Fig 1Ba, green fluorescence indicates that the anchoring strands (AS) are conjugated on the scaffolds surface through a DMA cross-linker. Blue fluorescence indicates that the complementary strands (CS) are linked with AMCA (Fig 1Bb), red fluorescence indicates that rhodamine-B labels the ECM (Fig 1Bc), and pink (red + blue) fluorescence indicates that the ECM is connected with the complementary strand (Fig 1Bd). The overlaid image shows that each part is stably joined and attaches to the scaffolds surface (Fig 1Be). These results suggest that the microscale BMSC-ECM can be successfully conjugated onto the 3D-HA scaffolds with the oligonucleotide immobilization system.

Scaffold Configuration and Basic Mechanical Properties

SEM was applied to analyse the surface and internal structure of the scaffolds. The two groups of scaffolds show a structure with multiple pores, smooth thin walls and connected apertures. Figure 2 shows the basic morphology of the scaffolds, the pore structure under SEM and the surface layers of the scaffolds. When combined with the micron-scale extracellular matrix, the composite scaffolds show a higher altitude (Figure 2F), which indicates that the scaffolds surface is covered with a biological layer.

3D reconstruction technology was applied to analyse the pore size, which is listed in Table 2. As the two groups of scaffolds applied the 3D-printed method, the internal structure is stable, with a consistent pore size. In addition, the mechanical properties of the 3D-HA scaffolds and composite scaffold are similar, and the compressive modulus are up to 9.45±0.32 MPa and 9.57±0.41 MPa. Moreover, after being fully immersed in the liquid, the mechanical properties of both scaffolds almost unchanged.

The computational dynamic fluid permeability simulation of the scaffolds showed that there is no obvious difference in current velocity on the surface of both scaffolds (Figure 3B and E). However, the velocity in the internal of the 3D-HA/BMSC-ECM scaffolds is obviously higher than C/G scaffolds (Figure 3A and D). In addition, the multi-layered analysis indicates that the 3D-HA/BMSC-ECM

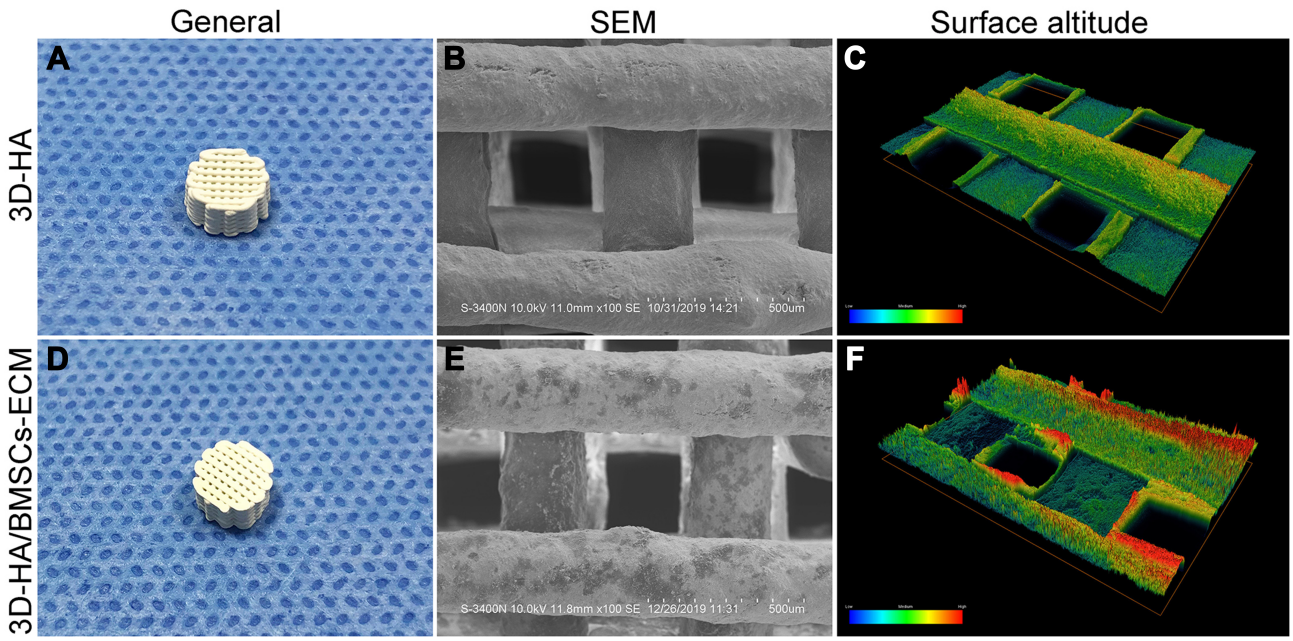

Figure 2 General morphology and surface characterization of the 3D-HA and 3D-HA/BMSC-ECM scaffolds. (**A**) General morphology, (**B**) SEM, and (**C**) surface altitude of the 3D-HA scaffold; (**D**) general morphology, (**E**) SEM, and (**F**) surface altitude of the 3D-HA/BMSC-ECM scaffold. Red indicates high altitude, and blue reflects low altitude.

scaffolds display a relative homogeneous and high velocity whether on the surface or inside, but for C/G scaffolds, the velocity of liquid is nonuniform, and the velocity inside the scaffolds is obviously lower than that on the surface (Figure 3C and F).

In vitro Cytotoxicity

The OD values are similar for the normal complete medium, the mixture with eluates from the 3D-HA scaffolds, and the mixture with 3-day eluate from the composite scaffolds. However, the OD values of the mixtures containing 5-day and 7-day eluates from the composite scaffolds are higher than the other groups (Figure 4A) ($P<0.01$). In addition, the proliferation ratio shows a similar trend (Figure 4B).

Cell Adhesion and Cytoactivity

The average cell adhesion ratio of the composite scaffolds after culturing 5 hours and 7 hours was 54.03±7.63% and 76.00±6.17%, which was much higher than that of the 3D-HA scaffolds ($P<0.05$ and 0.01). Figure 5A shows that after culturing for 3 and 7 days, fluorescence staining revealed that almost all cells in both scaffolds were green but more live cells were observed in the composite scaffolds after 7 days (Figure 5A). The cytoactivity of BMSCs on both scaffolds was also evaluated by SEM and cytoskeletal staining. For the SEM analysis, the cells on the 3D-HA/BMSC-ECM scaffolds grew vigorously and spread well and the ECM secreted by the cells almost covered the whole surface of the scaffolds. However, fewer cells adhered to the 3D-HA scaffolds and the cells poorly spread (Figure 5B). Cytoskeletal staining showed the same results as SEM for BMSCs on the 3D-HA scaffolds, which exhibited contracted or spindle shapes. On composite scaffolds, the BMSCs showed a clear cytoskeleton and a stretched morphology (Figure 5C). Figure 5D shows that although the two scaffolds displayed a similar cell adhesion ratio at 1 h and 3 h, the ratio of the

Table 2 Characteristics of the 3D-HA and 3D-HA/BMSC-ECM Scaffold

Scaffold	3D-HA	3D-HA/BMSC-ECM
Pore size (um)	315±34	305±47
Compressive modulus before immersed in liquid (MPa)	9.57±0.41	9.45±0.32
Compressive modulus after immersed in liquid (MPa)	9.47±0.33	9.39±0.46
Cell adhesion ratio after 7 h (%)	51.85±4.77	76.00±6.17

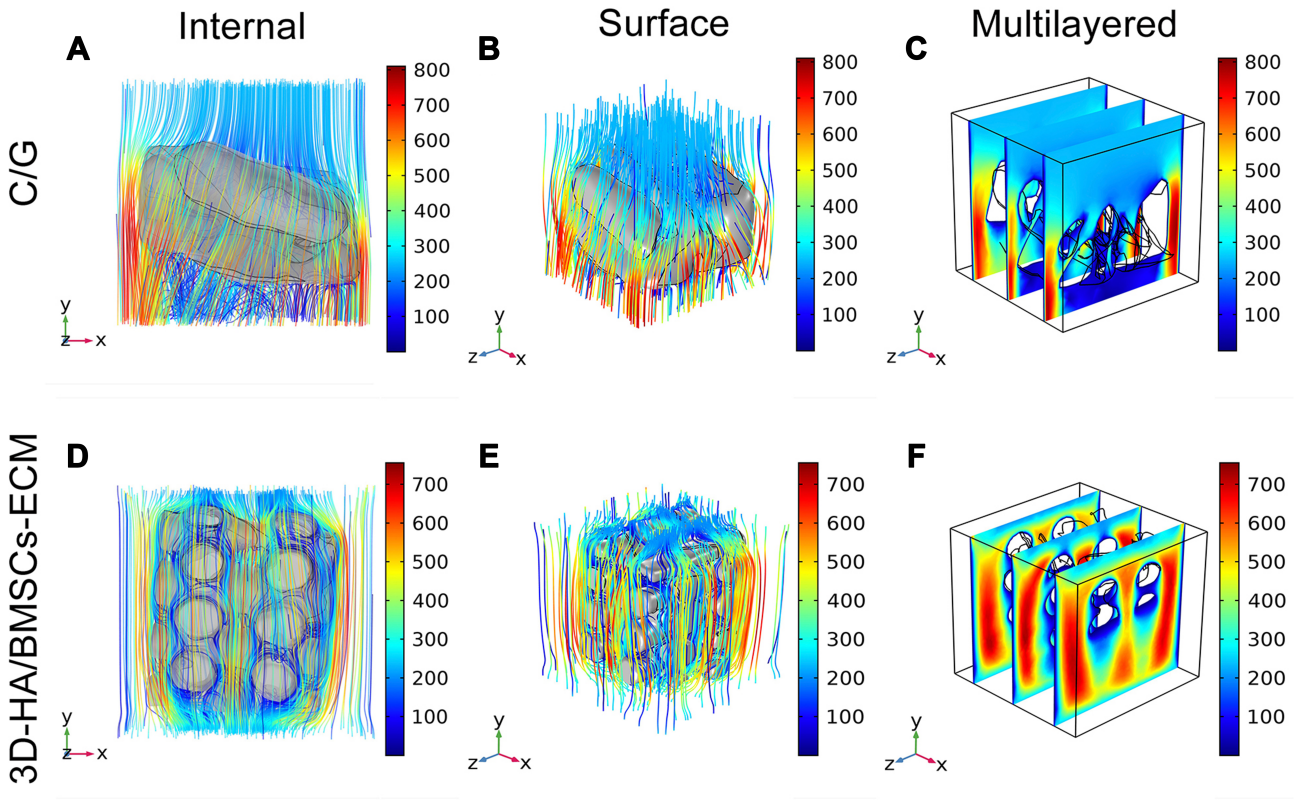

Figure 3 Computational dynamic fluid permeability simulation of the scaffolds. The (**A**) internal, (**B**) surface, and (**C**) multilayered analysis of C/G scaffold. The (**D**) internal, (**E**) surface, and (**F**) multilayered analysis of 3D-HA/BMSC-ECM scaffold. Red indicates high velocity and blue reflects low velocity (um/s).

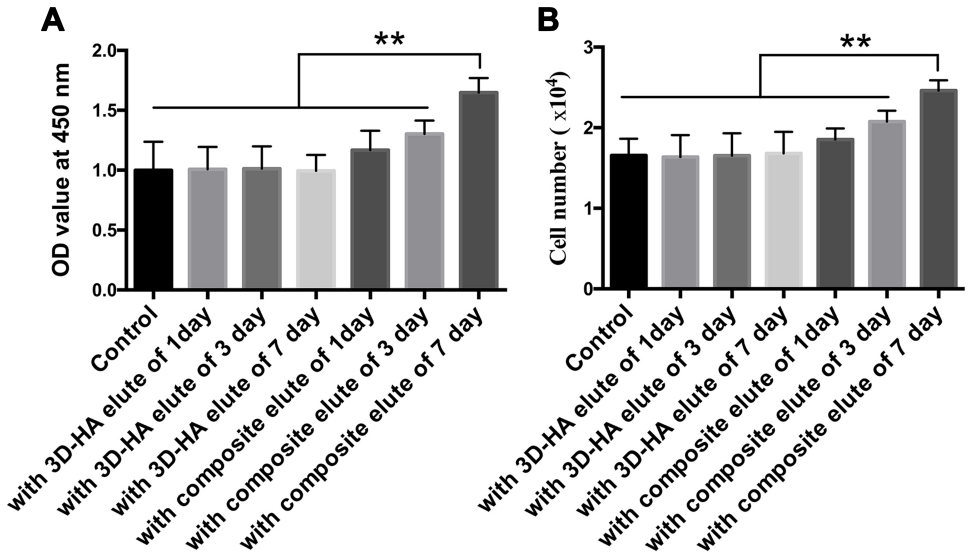

Figure 4 Cytotoxicity of the scaffolds. (**A**) OD value of the cells cultured with different elutes of scaffolds. (**B**) Proliferation ratio of BMSCs cultured with different scaffolds elutes. **P<0.01.

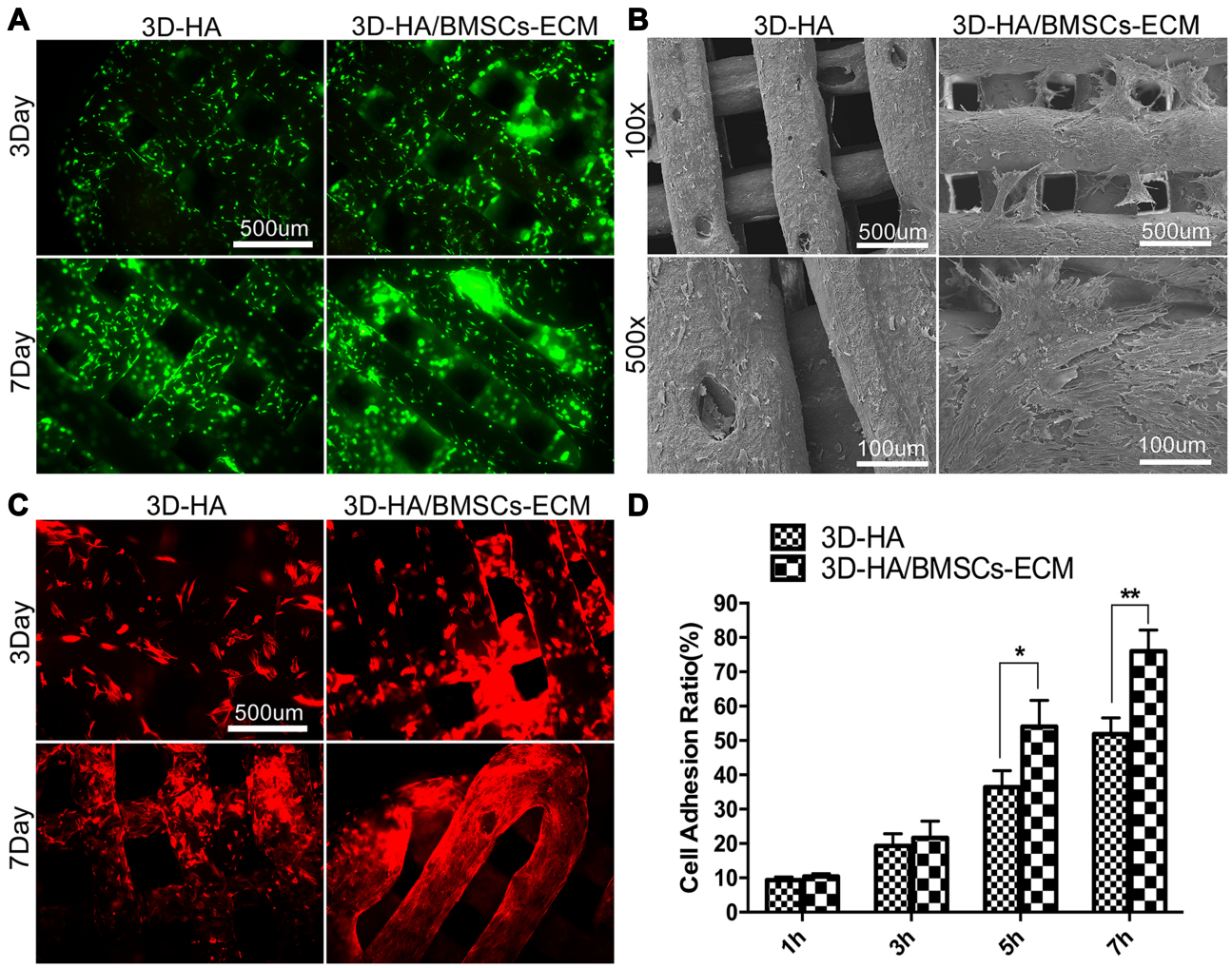

Figure 5 Cell adhesion, morphology and activity on different scaffolds. (**A**) live-dead staining. (**B**) SEM and (**C**) cytoskeleton staining show the morphology and activity of the BMSCs. (**D**) Cell adhesion ratio. *P<0.05, **P<0.01.

composite scaffold was significantly higher than that of the 3D-HA scaffolds at 5 h and 7 h.

3D-HA/BMSCS-ECM Scaffolds Promote Osteogenesis Induction in vitro

After culturing with normal complete medium and mixtures containing a 7-day eluate from both scaffolds, ALP was used to analyse the osteogenesis of BMSCs. BCIP/NBT staining showed that ALP staining significantly increased over time and the degree of staining was more pronounced in the composite scaffolds group than the 3D-HA scaffold group (Figure 6A). Another two staining methods, Alizarin red and von Kossa, showed similar trends as shown in Figure 6B.

In contrast, for the BMSCs cultured on scaffolds, Figure 6C shows the ALP activity with or without OS. With OS, the U value of the composite scaffolds reached a high level and increases with time. The U value of the 3D-HA scaffolds showed similar trend, although the value was much lower than that of the composite scaffolds at each time point (P<0.05). Without OS, the U value of 3D-HA scaffolds remained at a low level even after 3 weeks; however, for the composite scaffolds, the U value improved at 1 week, peaked at 2 weeks and was maintained until 3 weeks.

In addition, Figure 7 shows the RT-PCR results for Col I, ALP, OPN, OCN and Runx-2. The mRNA of ALP showed a trend similar to that of the ALP protein level. For Col I, with OS, the level of the composite scaffolds group reached a high level after 7 days and peaked after 14 days, with a level higher than that of the 3D-HA scaffolds group (P<0.01). After 21 days, it decreased and was lower than that in the 3D-HA scaffolds group (P<0.05). Without OS,

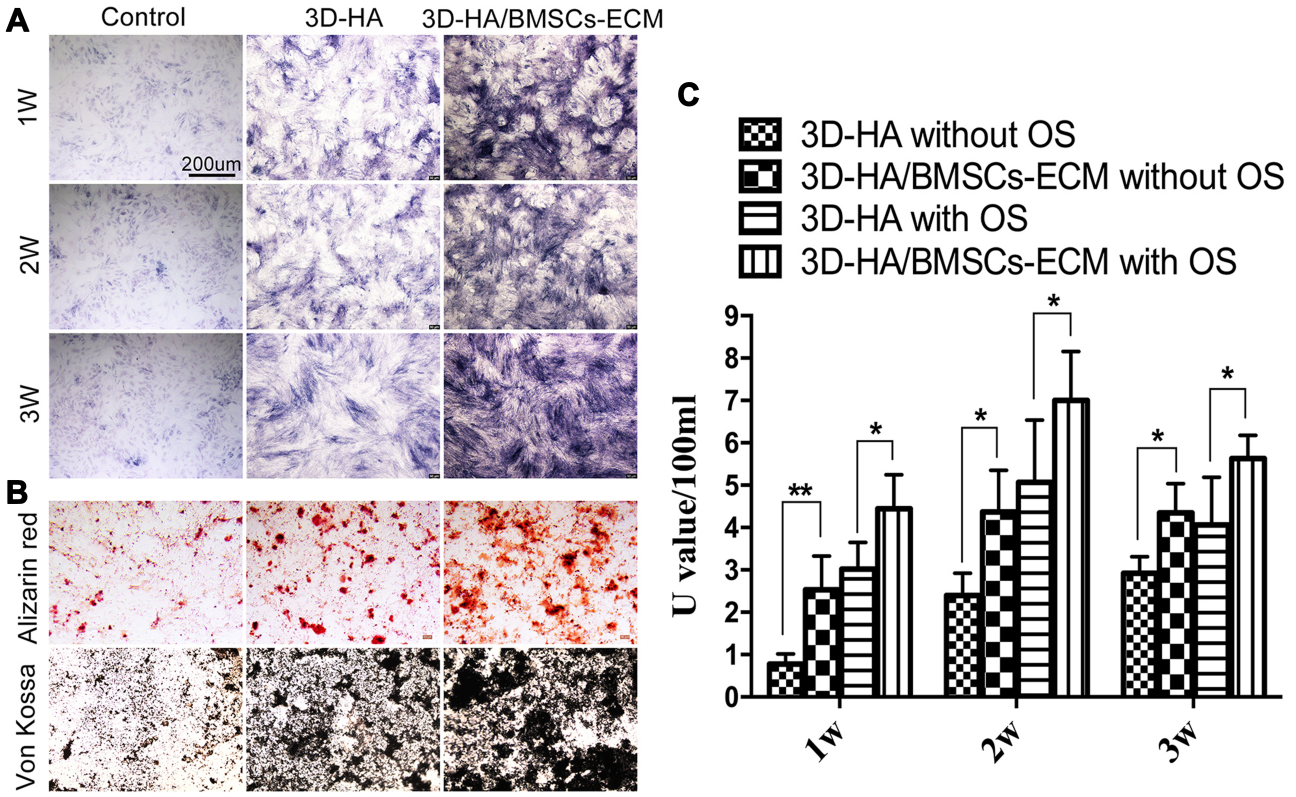

Figure 6 Osteogenic differentiation in vitro. (**A**) BCIP/NBT for ALP staining with different scaffolds elutes. (**B**) Alizarin red and Von Kossa staining with different scaffold elutes. (**C**) ALP activity of cells on different scaffolds. *P<0.05; **P<0.01.

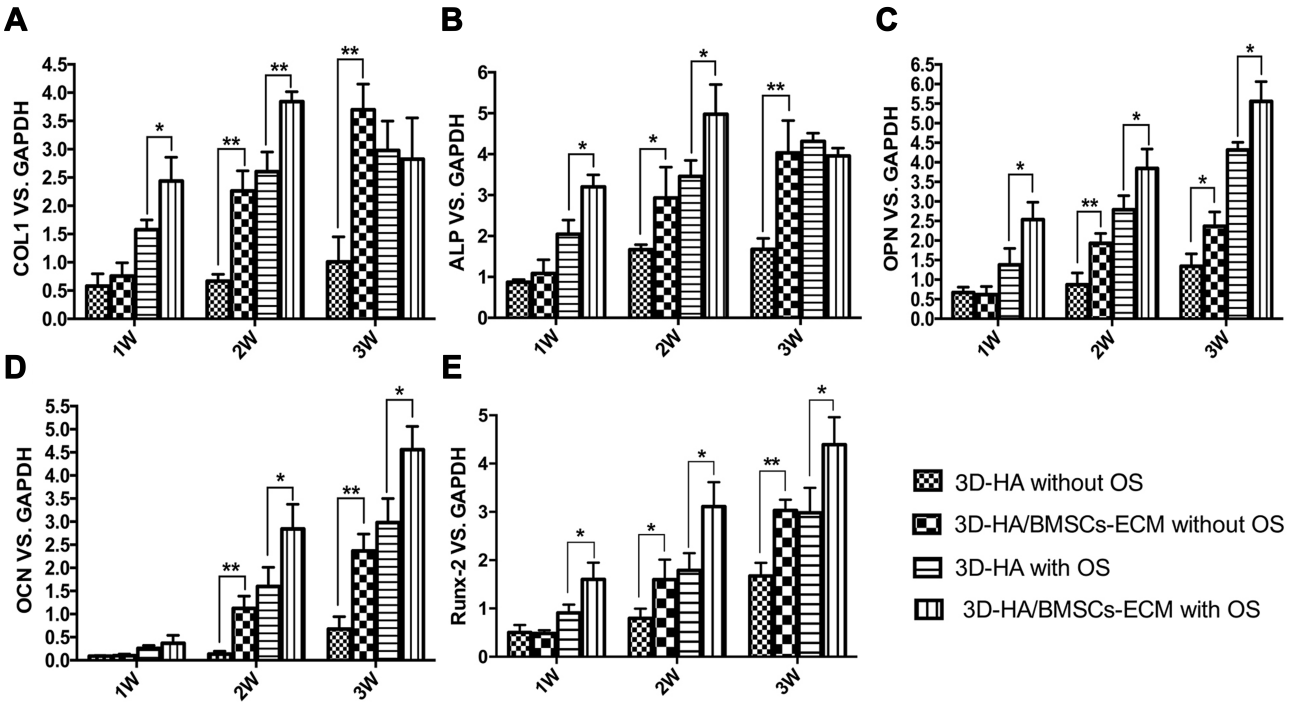

Figure 7 Osteogenic related mRNAs expression of BMSCs seeded on different scaffolds. (**A**) Col1, (**B**) ALP, (**C**) OPN, (**D**) OCN, (**E**)Runx-2. *P<0.05; **P<0.01.

the level of Col I mRNA increased with time in the composite scaffolds group and was much higher than that in the 3D-HA scaffolds group (P<0.05). The mRNA levels of OPN, OCN and Runx-2 all showed a similar trend, and the composite scaffolds group had a higher level than the 3D-HA scaffolds group with or without OS (P<0.05 or P<0.01).

3D-HA/BMSCS-ECM Scaffolds Accelerate the Repair of Critical Bone Defects

One rat in the blank control group and one rat in the composite scaffolds group died of unknown causes within 1 week, and the others recovered well. Twelve weeks after the operation, Micro-CT was used to assess the quality and quantity of bone repair. Better osteogenesis and osseointegration were observed in the composites scaffold group, while no obvious bone regeneration was observed in the 3D-HA scaffolds or control group (Figure 8A). In addition, BV/TV, Tb.N, Tb.Th and Tb.Sp were used to quantify osteogenesis, and the values were significantly higher in the composite scaffold group than those in the 3D-HA scaffold group and control group (Figure 8B–E). Thus, the 3D-HA/BMSC-ECM scaffolds can promote bone repair in vivo, which is consistent with the in vitro results.

Discussion

ECM contains various bioactive growth factors and has been increasingly applied to tissue engineering; however, its poor mechanical properties limit its applications.[29–32] Various kinds of techniques have been used for surface modification of different materials to improve the specific performance of the scaffold.[23] In this study, we prepared 3D-HA/BMSC-ECM composite scaffolds according to the surface modification of the 3D-HA scaffold using micron-scale ECM. First, the basic properties of the scaffolds were tested in vitro, and then their osteogenic ability was verified in vivo and in vitro.

As mentioned above, the physical properties of the scaffolds are very important, and the compressive strength of the composite scaffolds reaches 9.45±0.32 MPa, which is similar to that of the 3D-HA scaffolds. After being

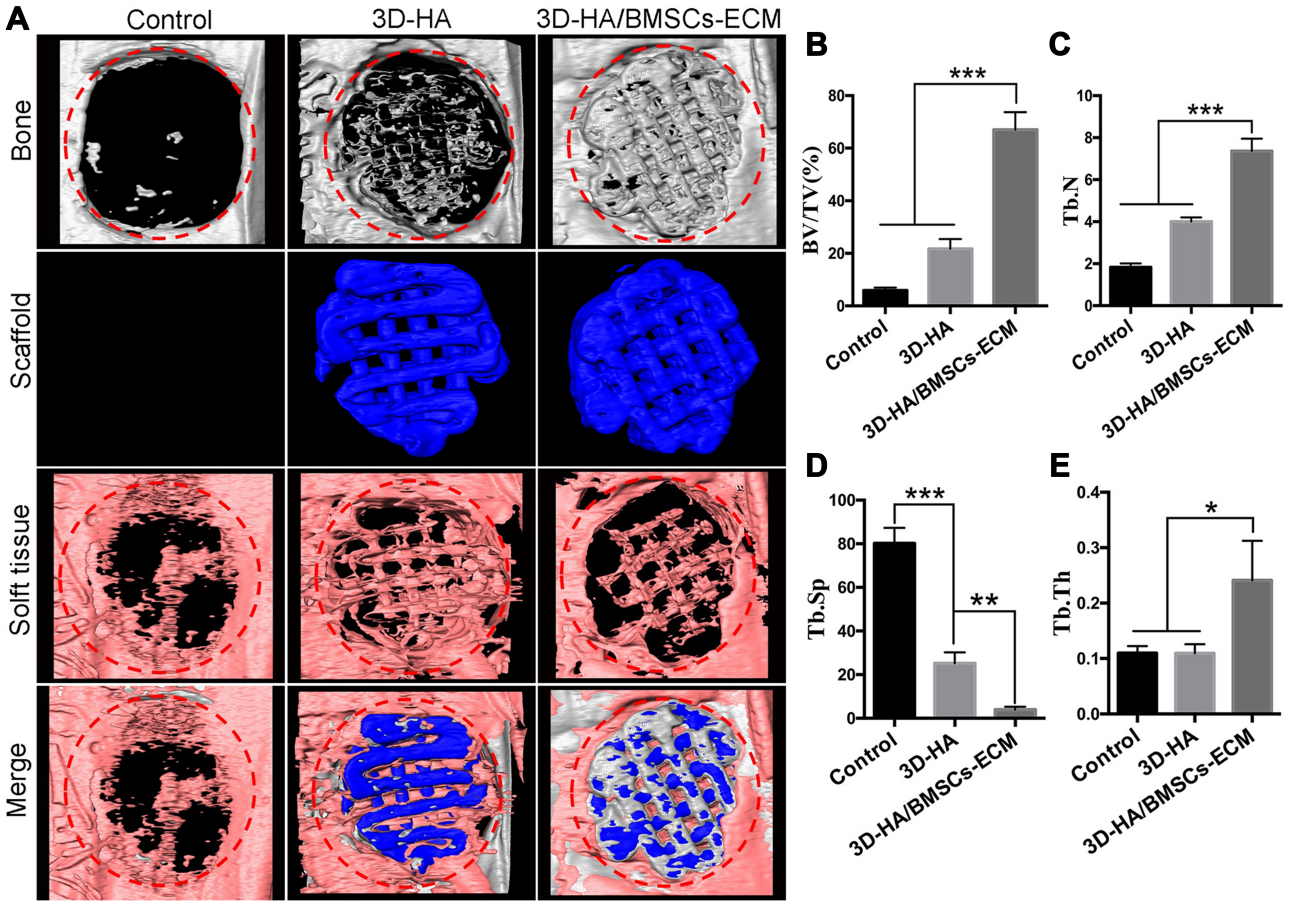

Figure 8 Radiographic analyze of bone repair after 3 months in a rat critical-size cranial defects mode. (**A**) Three-dimensional micro-CT reconstruction images of the defects. Quantity analysis of the new bone formation (**B**) BV/TV; (**C**)Tb.N; (**D**) Tb.Sp; and (**E**) Tb.Th. *P<0.05; **P<0.01; ***P<0.001.

soaked in water completely, their mechanics remained basically unchanged, which allows the scaffolds to retain sufficient mechanical strength after implantation. Previous studies have proven that stress is very important for cell proliferation;[2–5] therefore, the composite scaffolds are qualified candidates. In addition, because of the mature printing technology, the space inside the composite scaffolds is uniform, and computer hydrodynamics simulations have confirmed that the water distribution in composite scaffolds is even while that in the C/G scaffolds is obviously variable, which will lead to the presence of space in the C/G scaffolds without liquid passing through. In the application of scaffolds to promote osteogenesis, stem cells can be fully and evenly distributed in the composite scaffolds, while the distribution in the C/G scaffolds may be limited. In addition, the uniform interior pore structure is beneficial for the provision of nutrient sustenance and exclusion of metabolic waste in cells, which is necessary for cell proliferation,[33] and studies have confirmed that the optimal pore size for tissue engineering scaffolds is 100–350 μm.[34] In this experiment, the pore size of the 3D-HA scaffolds and composite scaffolds were approximately 350 microns and could be maintained for a long time in the body, which meets the requirements of osteogenic scaffolds.

In addition, in vitro toxicity tests and cell adhesion experiments have confirmed that the two scaffolds have no obvious cytotoxicity and do not inhibit cell proliferation, which is consistent with previous research. After 7 days, the composite scaffolds show more live cells and the vitality of cells adhered to the composite scaffolds is better, indicating that the ECM secreted by BMSCs has good activity and can significantly promote cell proliferation and adhesion.[2]

The cells on the composite scaffolds that display better cytoactivity and morphology than the cells on the control scaffolds may be ascribed to two reasons. First, the composite scaffolds show a better adhesion ratio than the 3D-HA scaffolds. Cell adhesion is the first step of the cell–scaffold interaction, and better adhesion is more beneficial for subsequent proliferation and extracellular matrix formation. Secondly, the surface of the composite scaffolds is covered by ECM, and ECM has several kinds of functional proteins that are beneficial for cell growth.[35–38]

We then further demonstrated the osteogenic capacity of the scaffolds in vivo and in vitro. We collected the eluates of the different scaffolds and applied them to the BMSC culture. We found that the secretion of ALP with composite scaffolds elutes was significantly stronger than that induced by control scaffolds elutes and normal medium, and the calcium nodules generated by cell mineralization significantly increased, indicating that the component contained in ECM had a strong ability to induce osteogenic differentiation. After cells adhered onto the scaffolds, the BMSCs/scaffolds were cultured with or without osteogenesis induction. The ALP protein is a classical marker of bone formation; in composite scaffolds with OS, it can reach a high level after 7 days and peak after 14 days and is maintained until 21 days, which is significantly higher than that of control scaffolds. Without OS, it can also reach a high level after 21 days in composite scaffolds, while the control scaffolds were significantly worse. For osteoblastic marker mRNAs, we chose Col I, ALP, OPN, OCN, and Runx-2 because Col I and ALP are markers of early osteogenesis, OPN is a marker of middle osteogenesis, OCN is a marker of late osteogenesis,[39,40] and Runx-2 is another classic marker of osteogenesis, which supports osteogenesis detection covering the whole osteogenesis process.[41,42] However, because the calcium nodules generated by cell mineralization are close to HA nodules, the newly generated calcium nodules cannot be stained for analysis.

We established a model of skull defect in rats, and after 3 months, there was no significant bone regeneration at the defect site, confirming that the model of critical bone defects was successfully established. The osteogenesis effects of the 3D-HA and composite scaffolds were also evaluated, and after 3 months, the bone repair in 3D-HA group was much worse, which may have been related to the weaker osteogenic induction ability. However, the composite scaffolds exhibited better bone-scaffold integration and new bone appeared on and around the scaffolds, which indicated the bioactive function of BMSC-ECM and the great potential of composite scaffold for bone regeneration.

Conclusions

In summary, BMSC-ECM is an organic material with a strong osteogenic ability. After modifying the surface of the 3D-HA scaffolds, the composite scaffolds show a good tissue-space structure and good osteogenic performance and have great application potential. However, due to the complexity of the BMSC-ECM components and functions, it is still difficult to identify the specific mechanism of BMSC-ECM osteogenesis; thus, further research is needed in the future.

Funding

This study was supported by the Natural Science Foundation of Heilongjiang Province, China (Grant No. YQ2019H008) and Innovative Science Research Fund of Harbin Medical University.

Disclosure

The authors report no conflicts of interest for this work.

References

1. Seok JM, Rajangam T, Jeong JE, et al. Fabrication of 3D plotted scaffold with microporous strands for bone tissue engineering. *J Mater Chem B*. 2020;8(5):951–960. doi:10.1039/c9tb02360g
2. Wang X, Yu T, Chen G, Zou J, Li J, Yan J. Preparation and characterization of a chitosan/gelatin/extracellular matrix scaffold and its application in tissue engineering. *Eng Part C Methods*. 2017;23 (3):169–179. doi:10.1089/ten.TEC.2016.0511
3. Chan KH, Zhuo S, Ni M. Natural and synthetic peptide-based biomaterials for bone tissue engineering. *OA Tissue Eng*. 2013;1(6):1–5. doi:10.13172/2052-9643-1-1-787
4. Yang C, DelRio FW, Ma H, et al. Spatially patterned matrix elasticity directs stem cell fate. *Proc Natl Acad Sci U S A*. 2016;113(31): E4439–45. doi:10.1073/pnas.1609731113
5. Przybyla L, Lakins JN, Weaver VM. Tissue mechanics orchestrate wnt-dependent human embryonic stem cell differentiation. *Cell Stem Cell*. 2016;19(4):462–475. doi:10.1016/j.stem.2016.06.018
6. Dong L, Gong J, Wang Y, et al. Chiral geometry regulates stem cell fate and activity. *Biomaterials*. 2019;222:119456. doi:10.1016/j.biomaterials.2019.119456
7. Chan KH, Lee WH, Zhuo S, Ni M. Harnessing supramolecular peptide nanotechnology in biomedical applications. *Int J Nanomedicine*. 2017;12:1171–1182. doi:10.2147/IJN.S126154
8. Midwood KS, Williams LV, Schwarzbauer JE. Tissue repair and the dynamics of the extracellular matrix. *Int J Biochem Cell Biol*. 2004;36(6):1031–1037. doi:10.1016/j.biocel.2003.12.003
9. Reilly GC, Engler AJ. Intrinsic extracellular matrix properties regulate stem cell differentiation. *J Biomech*. 2010;43(1):55–62. doi:10.1016/j.jbiomech.2009.09.009
10. Harvestine JN, Orbay H, Chen JY, Sahar DE, Leach JK. Cell-secreted extracellular matrix, independent of cell source, promotes the osteogenic differentiation of human stromal vascular fraction. *J Mater Chem B*. 2018;6(24):4104–4115. doi:10.1039/C7TB02787G
11. Wang X, Chen G, Huang C, Tu H, Zou J, Yan J. Bone marrow stem cells-derived extracellular matrix is a promising material. *Oncotarget*. 2017;8(58):98336–98347. doi:10.18632/oncotarget.21683
12. Amani H, Mostafavi E, Arzaghi H, et al. Three-dimensional graphene foams: synthesis, properties, biocompatibility, biodegradability, and applications in tissue engineering. *ACS Biomater Sci Eng*. 2019;5 (1):193–214. doi:10.1021/acsbiomaterials.8b00658
13. Xu HH, Wang P, Wang L, et al. Calcium phosphate cements for bone engineering and their biological properties. *Bone Res*. 2017;5 (1):17056. doi:10.1038/boneres.2017.56
14. Hong N, Yang GH, Lee J, Kim G. 3D bioprinted and its in vivo applications. *J Biomed Mater Res B Appl Biomater*. 2018;106 (1):444–459. doi:10.1002/jbm.b.33826
15. Pina S, Ribeiro VP, Marques CF, et al. Scaffolding strategies for tissue engineering and regenerative medicine applications. *Materials (Basel)*. 2019;12(11):E1824. doi:10.3390/ma12111824
16. Chan KH, Zhuo S, Ni M. Priming the surface of orthopedic implants for osteoblast attachment in bone tissue engineering. *Int J Med Sci*. 2015;12(9):701–707. doi:10.7150/ijms.12658
17. Akkineni AR, Luo Y, Schumacher M, Nies B, Lode A, Gelinsky M. 3D plotting of growth factor loaded calcium phosphate cement scaffold. *Acta Biomater*. 2015;27:264–274. doi:10.1016/j.actbio.2015.08.036
18. Wang H, Wu G, Zhang J, et al. Osteogenic effect of controlled released rhBMP-2 in 3D printed porous hydroxyapatite scaffold. *Colloids Surf B Biointerfaces*. 2016;141:491–498. doi:10.1016/j.colsurfb.2016.02.007
19. Lee SJ, Lee D, Yoon TR, et al. Surface modification of 3D-printed porous scaffold via mussel-inspired polydopamine and effective immobilization of rhBMP-2 to promote osteogenic differentiation for bone tissue engineering. *Acta Biomater*. 2016;40:182–191. doi:10.1016/j.actbio.2016.02.006
20. Carvalho MS, Silva JC, Cabral JMS, da Silva CL, Vashishth D. Cultured cell-derived extracellular matrices to enhance the osteogenic differentiation and angiogenic properties of human mesenchymal stem/stromal cells. *J Tissue Eng Regen Med*. 2019;13 (9):1544–1558. doi:10.1002/term.2907
21. CHarvestine JN, Vollmer NL, Ho SS, Zikry CA, Lee MA, Leach JK. Extracellular matrix-coated composite scaffolds promote mesenchymal stem cell persistence and osteogenesis. *Biomacromolecules*. 2016;17(11):3524–3531. doi:10.1021/acs.biomac.6b01005
22. Wang S, Wen S, Shen M, Guo R, Cao X, Wang J. Aminopropyltriethoxysilane-mediated surface functionalization of hydroxyapatite nanoparticles: synthesis, characterization, and in vitro toxicity assay. *Int J Nanomedicine*. 2011;6:3449–3459. doi:10.2147/IJN.S27166
23. Amani H, Arzaghi H, Bayandori M, et al. Controlling cell behavior through the design of biomaterial surfaces: a focus on surface modification techniques (open access in wiley.com, hall of fame article). *Adv Mater Interfaces*. 2019;6(13):1900572. doi:10.1002/admi.201900572
24. Chen G, Sun Y, Lu F, et al. A three-dimensional (3D) printed biomimetic hierarchical scaffold with a covalent modular release system for osteogenesis. *Mater Sci Eng C Mater Biol Appl*. 2019;104:109842. doi:10.1016/j.msec.2019.109842
25. Beutner R, Michael J, Förster A, Schwenzer B, Scharnweber D. Immobilization of oligonucleotides on titanium based materials by partial incorporation in anodic oxide layers. *Biomaterials*. 2009;30 (14):2774–2781. doi:10.1016/j.biomaterials.2009.01.047
26. Gaebler A, Schaefer T, Fischer K, Scharnweber D, Mauth C, Schwenzer B. Peptide linkers for the immobilization of bioactive molecules on biphasic calcium phosphate via a modular immobilization system. *Acta Biomater*. 2013;9(1):4899–4905. doi:10.1016/j.actbio.2012.08.025
27. Xu Y, Xu GY, Tang C, et al. Preparation and characterization of bone marrow mesenchymal stem cells-derived extracellular matrix scaffold. *J Biomed Mater Res B Appl Biomater*. 2015;103 (3):670–678. doi:10.1002/jbm.b.33231
28. Gómez S, Vlad MD, López J, Fernández E. Design and properties of 3D scaffold for bone tissue engineering. *Acta Biomater*. 2016;42:341–350. doi:10.1016/j.actbio.2016.06.032
29. Li YM, Wu JY, Jiang J, et al. Chondroitin sulfate-polydopamine modified polyethylene terephthalate with extracellular matrix-mimetic immunoregulatory functions for osseointegration. *J Mater Chem B*. 2019;7(48):7756–7770. doi:10.1039/c9tb01984g
30. Yu Z, Lili J, Tiezheng Z, et al. Development of decellularized meniscus extracellular matrix and gelatin/chitosan scaffolds for meniscus tissue engineering. *Bio Med Mater Eng*. 2019;30 (2):125–132. doi:10.3233/BME-191038
31. Li W, Midgley AC, Bai Y, et al. Subcutaneously engineered autologous extracellular matrix scaffold with aligned microchannels for enhanced tendon regeneration: aligned microchannel scaffold for tendon repair. *Biomaterials*. 2019;224:119488. doi:10.1016/j.biomaterials.2019.119488

32. Liu Y, Kuang B, Rothrauff BB, Tuan RS, Lin H. Robust bone regeneration through endochondral ossification of human mesenchymal stem cells within their own extracellular matrix. *Biomaterials*. 2019;218:119336. doi:10.1016/j.biomaterials.2019.119336
33. Ji C, Annabi N, Khademhosseini A, Dehghani F. Fabrication of porous chitosan scaffold for soft tissue engineering using dense gas CO2. *Acta Biomater*. 2011;7(4):1653–1664. doi:10.1016/j.actbio.2010.11.043
34. Whang K, Healy KE, Elenz DR, et al. Engineering bone regeneration with bioabsorbable scaffold with novel microarchitecture. *Tissue Eng*. 1999;5(1):35–51. doi:10.1089/ten.1999.5.35
35. McDevitt CA, Wildey GM, Cutrone RM. Transforming growth factor-beta1 in a sterilized tissue derived from the pig small intestine submucosa. *J Biomed Mater Res A*. 2003;67(2):637–640. doi:10.1002/jbm.a.10144
36. Lai Y, Sun Y, Skinner CM, et al. Reconstitution of marrow-derived extracellular matrix ex vivo: a robust culture system for expanding large-scale highly functional human mesenchymal stem cells. *Stem Cells Dev*. 2010;19(7):1095–1107. doi:10.1089/scd.2009.0217
37. Carvalho MS, Silva JC, Udangawa RN, et al. Co-culture cell-derived extracellular matrix loaded electrospun microfibrous scaffold for bone tissue engineering. *Mater Sci Eng C Mater Biol Appl*. 2019;99:479–490. doi:10.1016/j.msec.2019.01.127
38. CSilva JC, Carvalho MS, Udangawa RN, et al. Extracellular matrix decorated polycaprolactone scaffold for improved mesenchymal stem/stromal cell osteogenesis towards a patient-tailored bone tissue engineering approach. *J Biomed Mater Res B Appl Biomater*. 2020. doi:10.1002/jbm.b.34554
39. Osyczka AM, Leboy PS. Bone morphogenetic protein regulation of early osteoblast genes in human marrow stromal cells is mediated by extracellular signal-regulated kinase and phosphatidylinositol 3-kinase signaling. *Endocrinology*. 2005;146(8):3428–3437. doi:10.1210/en.2005-0303
40. Zou J, Yuan C, Wu C, Cao C, Yang H. The effects of platelet-rich plasma on the osteogenic induction of bone marrow mesenchymal stem cells. *Connect Tissue Res*. 2014;55(4):304–309. doi:10.3109/03008207.2014.930140
41. Lin H, Yang G, Tan J, Tuan RS. Influence of decellularized matrix derived from human mesenchymal stem cells on their proliferation, migration and multi-lineage differentiation potential. *Biomaterials*. 2012;33(18):4480–4489. doi:10.1016/j.biomaterials.2012.03.012
42. Bae SE, Bhang SH, Kim BS, Park K. Self-assembled extracellular macromolecular matrices and their different osteogenic potential with preosteoblasts and rat bone marrow mesenchymal stromal cells. *Biomacromolecules*. 2012;13(9):2811–2820. doi:10.1021/bm300791h